Current Biology 20, 1993–2002, November 23, 2010 ©2010 Elsevier Ltd All rights reserved DOI 10.1016/j.cub.2010.09.063

Article

WNT5A/JNK and FGF/MAPK Pathways Regulate the Cellular Events Shaping the Vertebrate Limb Bud

Jerome Gros,[1] Jimmy Kuang-Hsien Hu,[1] Claudio Vinegoni,[2] Paolo Fumene Feruglio,[2,3] Ralph Weissleder,[2] and Clifford J. Tabin[1,*]

[1]Department of Genetics, Harvard Medical School, 77 Avenue Louis Pasteur, Boston, MA 02115, USA

[2]Center for Systems Biology, Massachusetts General Hospital, Harvard Medical School, 185 Cambridge Street, Boston, MA 02114, USA

[3]Department of Neurological, Neuropsychological, Morphological and Movement Sciences, University of Verona, Strada Le Grazie 8, 37134 Verona, Italy

Summary

Background: The vertebrate limb is a classical model for understanding patterning of three-dimensional structures during embryonic development. Although decades of research have elucidated the tissue and molecular interactions within the limb bud required for patterning and morphogenesis of the limb, the cellular and molecular events that shape the limb bud itself have remained largely unknown.

Results: We show that the mesenchymal cells of the early limb bud are not disorganized within the ectoderm as previously thought but are instead highly organized and polarized. Using time-lapse video microscopy, we demonstrate that cells move and divide according to this orientation. The combination of oriented cell divisions and movements drives the proximal-distal elongation of the limb bud necessary to set the stage for subsequent morphogenesis. These cellular events are regulated by the combined activities of the WNT and FGF pathways. We show that WNT5A/JNK is necessary for the proper orientation of cell movements and cell division. In contrast, the FGF/MAPK signaling pathway, emanating from the apical ectodermal ridge, does not regulate cell orientation in the limb bud but instead establishes a gradient of cell velocity enabling continuous rearrangement of the cells at the distal tip of the limb.

Conclusions: Together, these data shed light on the cellular basis of vertebrate limb bud morphogenesis and uncover new layers to the sequential signaling pathways acting during vertebrate limb development.

Introduction

The vertebrate limb bud forms as a mound of cells slightly elongated along the rostrocaudal axis of the embryo. As it grows, the early limb bud rapidly transforms into a paddle shape with an extended proximal-distal axis. Attaining this shape of the progenitor field is critical for producing limb segments and skeletal elements of the correct size and shape.

One previous model proposed to account for the proximal-distal directional elongation of the early limb mesenchyme based on differential proliferation rates between the proximal- and distalmost ends of the limb bud. This view posits that a higher proliferation rate at the distal end of the limb bud could act to ensure a proximal-distal oriented outgrowth [1]. Although a number of computational models have suggested that this mechanism could in principle account for observed changes in the shape of the limb bud [1–3], several studies have reported that proliferation is uniform throughout the mesenchyme during limb development and that only at late stages can an increase in proliferation be seen in the digital tips (from stage 23–25 in the chick and from E12.5 in the mouse) [4–6]. At these stages, the limb has already acquired its overall elongated shape. Thus, because proliferation appears to be largely isotropic at early stages, it cannot account for the dramatic changes observed in the shape of the limb bud.

An alternative hypothesis to explain how the limb acquires its shape involves oriented rearrangements of mesenchymal cells. This hypothesis was proposed in the early 1970s by Hornbruch and Wolpert when they were unable to identify differential proliferation within the developing limb bud [4]. However, at the time, tools were not available to test the veracity of this hypothesis in the context of the limb bud. Here, we brought powerful imaging methods to bear on the question of how the early limb primordium attains the shape required to serve as a substrate for patterning and to potentiate limb morphogenesis.

Results

Characterization of Chick Limb Elongation

To understand the mechanisms that might be involved in limb elongation, we first characterized it at the tissue level. Using optical projection tomography, we were able to accurately measure all three axes of the limb (anterior-posterior [A-P], dorsal-ventral [D-V], and proximal-distal [P-D]). Axis measurements were performed on 3D reconstructed limbs of chick embryos at Hamburger-Hamilton (HH) stages 18, 20, 21, and 23, which cover ~24–30 hr of development (Figures 1A–1H; see also Movie S1 available online). As expected, we found that during this time window, the P-D axis length increased dramatically (about three times). Surprisingly, we found that the D-V axis length did not increase much, and the A-P axis length actually decreased (Figure 1I). Because cells in the limb mesenchyme have been previously shown to uniformly proliferate at these stages [1, 4, 6], one would have expected all three axes to increase in length. The fact that the P-D axis is the only one to dramatically increase in length suggests that differential rates in isotropic proliferation cannot explain limb shape. Cell death has been extensively studied in this context and has been shown to play a role in refining the limb shape at later stages of this process. Although cell death, known to be present in the proximal anterior and posterior part of the limb bud, can explain the decrease in length of the A-P axis [6], it cannot account for the absence of major growth of the D-V axis. Thus, this analysis strongly suggests that other oriented mechanisms within the limb bud must act to accentuate its growth preferentially along the P-D axis.

Mesenchymal Cells of the Limb Bud Are Oriented

The early limb bud is generally conceptualized as an ectodermal bag containing a mound of uniformly distributed and

*Correspondence: tabin@genetics.med.harvard.edu

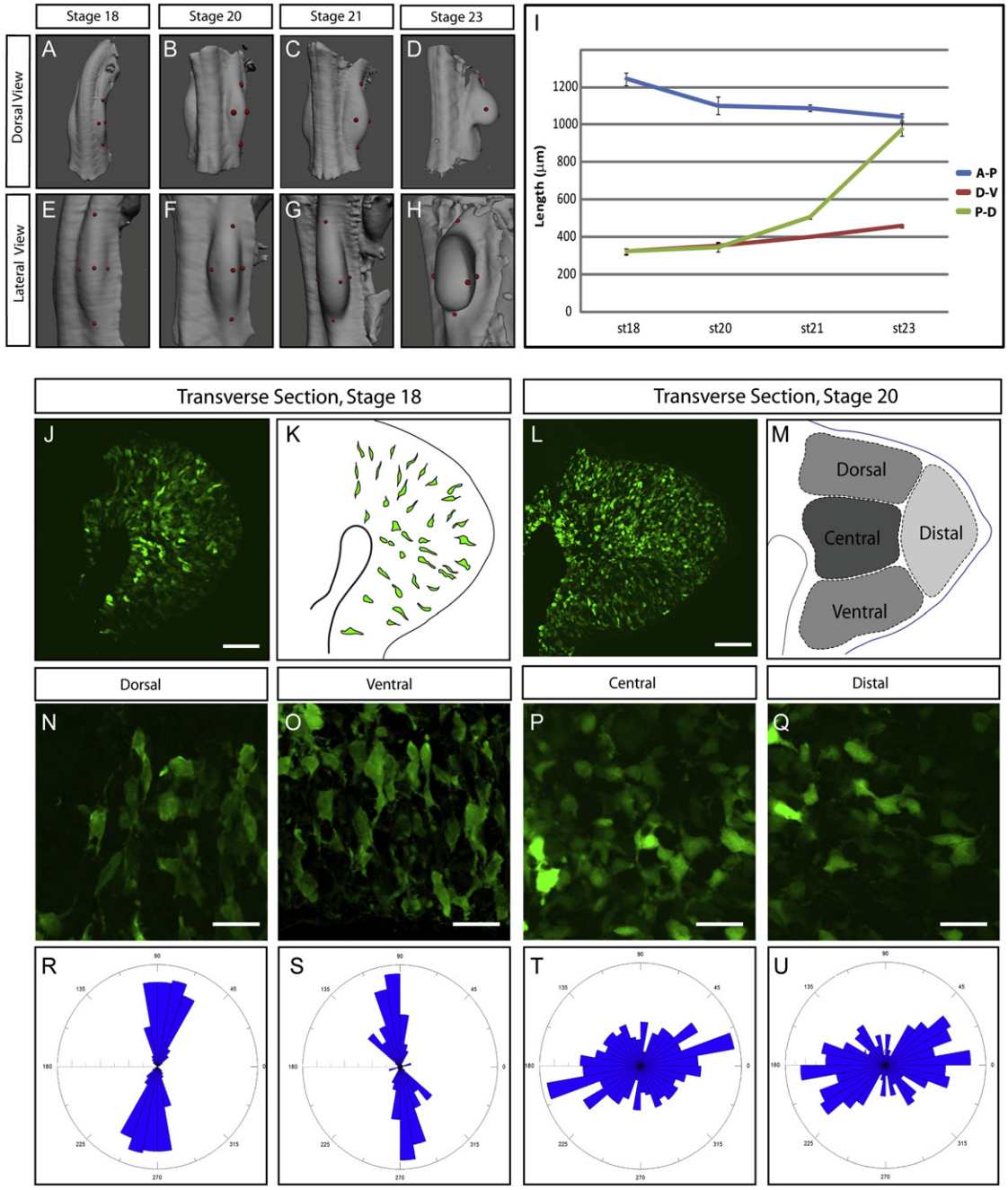

Figure 1. Characterization of Limb Bud Elongation at the Tissue and Cellular Level

(A–H) Three-dimensional reconstructions of optical projection tomography (OPT) acquisitions at the level of the limb bud of chick embryos at Hamburger-Hamilton (HH) stages 18 (A and E), 20 (B and F) 21 (C and G), and 23 (D and H) showing dorsal (A–D) and lateral (E–H) views. The red dots indicate where measurements were made. (See Movie S1.)

(I) Measurements of the length (in μm) of the anterior-posterior (A-P, blue line), dorsal-ventral (D-V, red line), and proximal-distal (P-D, green line) axes show that the limb bud elongates primarily on the P-D axis. A minimum of n = 8 limbs were analyzed for each time point. Error bars represent standard errors of the mean.

(J) Transverse section of an electroporated chick embryo at stage HH18 revealing the shape of *GFP*-expressing cells.

(K) Schematic representing the section shown in (D). A few *GFP*-expressing cells have been outlined to show their orientation and elongated shape.

(L) Transverse section of an electroporated embryo at stage 20 showing the shape of *GFP*-expressing cells (in green).

(M) Schematic representing four regions (dorsal, ventral, central, and distal) of the section shown in (L).

(N–Q) Enlargements of the dorsal (N), ventral (O), central (P), and distal (Q) limb bud regions of a chick embryo at stage HH21 showing the shape of the *GFP*-expressing cells.

(R–U) Quantification of the angle between the P-D axis of the limb bud and the longest axis of *GFP*-expressing cells observed in the dorsal (R), ventral (S), central (T), and distal (U) regions at stage HH21. Angle of each cell's longest axis is shown on a bidirectional rosette graph divided into bins of 5°. Each interval on the radial axis in (R)–(T) represents five cells per bin; each interval on the radial axis in (U) represents two cells per bin. Quantifications were made for a total of n = 1468 cells with a minimum of n = 300 cells for each area.

Scale bars represent 50 μm in (J) and (L) and 20 μm in (N)–(Q).

randomly arranged mesenchymal cells. However, we reasoned that if there were oriented cellular processes in the limb bud, they should be reflected in the organization of the mesenchymal cells themselves. To this end, we electroporated a *GFP* reporter gene into the early chick limb mesoderm. Because not all the cells incorporate the plasmid DNA carrying the transgene, the shape of the cells becomes easily observable (Figures 1J and 1L). Strikingly, we found that at about stage 18, cells were not disorganized. Mesenchymal cells displayed an apparent radial orientation, such that they were elongated and bipolar with protrusions in the direction of the overlying ectoderm (Figures 1J and 1K). At later stages (stage 20, Figure 1L, and stage 23, not shown), cells still displayed an orientation but exhibited regional differences (Figures 1L and 1M). At stage 20, quantifications showed that cells located in the ventral and dorsal sides close to the ectoderm (in about a 100 μm range) were greatly elongated (length/width [L/W] = 4, standard error of the mean [SEM] = 0.081, n = 304 cells and L/W = 3.7, SEM = 0.009, n = 568 cells, respectively) and were aligned perpendicular to the ectoderm (Figures 1N, 1R, 1O, and 1S). Cells located distally, close to the apical ectodermal ridge (AER), appeared to be oriented toward the ectoderm but were not as elongated (L/W = 1.87, SEM = 0.004, n = 302; Figures 1Q and 1U), whereas cells located centrally did not show evidence of organization and did not appear to be elongated (L/W = 1.5, SEM = 0.002, n = 308; Figures 1P and 1T).

Live Imaging Reveals Oriented Cell Movements and Oriented Division in the Limb Mesenchyme

We next utilized time-lapse microscopy to investigate how this organization arises. *GFP*-electroporated chick embryos were transversally sectioned (200 μm thick) with a vibratome, and selected sections encompassing *GFP*-labeled limbs were cultured under a controlled atmosphere and examined via two-photon microscopy. Explants were kept in culture on average 12 to 15 hr, and an image was taken every 3–5 min (Figure 2A; Movie S2). We found that labeled cells moved actively within the limb mesenchyme. These movements exhibited several characteristics. First, the movements of cells showed a clear directionality and, as predicted by the cell shape analysis, cells moved toward the overlying ectoderm (Figures 2B and 2C). Oriented protrusions described above were found to be persistent and very stable; cells appeared to use them to pull themselves toward the ectoderm. Second, we noted a gradient in cell velocity, with cells located distally moving faster than cells located more proximally (Figure 2D). Third, we also noted a gradient in the degree of coordination of movements. This was quantified by measuring the degree of coherence (similarity in trajectory of adjacent cells [7]) and efficiency (linearity of trajectory) of cell movement. We found that cells located close to the ectoderm moved more coherently and more efficiently (as defined by the ratio of the net movement over the total displacement) than cells located more proximally (Figure 2D). Thus, this analysis reveals that cells composing the early limb mesenchyme constantly rearrange through highly organized movements.

As cells moved toward the ectodermal layer, we noted that they tended to divide such that daughter cells separated along the direction of their movements (i.e., in direction of the ectoderm; Figures 2E, 2F, and 2H–2J; Movie S2; Movie S3). We quantified this result and found that overall, mesenchymal cells divided preferentially along the P-D axis (Figure 2G). It is important to note that in the dorsal and ventral part of the limb, cells divided with a greater angle in relation to the P-D axis (i.e., closer to the D-V axis). Interestingly, in these regions we noted that in many cases over the course of the time-lapse experiment, daughter cells that were pushed proximally reintercalated via the oriented movements described above. Thus, the oriented movements allow the intercalation of newly generated daughter cells perpendicular to the ectoderm, ensuring the elongation of the limb bud along its P-D axis. Altogether, these data show that the limb bud elongates via the combination of oriented cell division and oriented movements.

Wnt5a Regulates Cell Organization and Cell Movement in the Mouse Limb Bud

The WNT/planar cell polarity (PCP) pathway has been shown to regulate both oriented movement and cell division in developing embryos (for review, see [8]). Thus, this pathway was an obvious candidate for regulating the oriented events taking place in limb development. Interestingly, it is known that *Wnt5a* is expressed in a proximal-to-distal gradient within mesenchyme as well as in the distal ectoderm from as early as E9.5 in the mouse and as early as stage 18 in the chick limb bud ([9–11] and Figure 3A). Moreover, mice mutant for *Wnt5a* exhibit strong limb morphogenesis defects with shortened and malformed skeletal elements [11]. This phenotype, which does not involve specification or patterning defects, had been proposed to be due to a decrease in proliferation. However, in light of our cellular data, we decided to reexamine limbs of *Wnt5a* mutant embryos. We first quantified limb axis proportions in wild-type (WT) and $Wnt5a^{-/-}$ mouse E10.5 embryos using optical projection tomography (Figures 3A and 3B). We found that mutant limbs exhibited a 10% decrease in volume (data not shown), a result consistent with the previously described decrease in proliferation [11]. However, we found that the relative proportions of the *Wnt5a* mutant limbs were also affected. Limbs of $Wnt5a^{-/-}$ embryos exhibited a slight decrease in the length of A-P axis, a much greater decrease in their P-D axis, and more surprisingly, an increase in the length of the D-V axis when compared to WT littermates (Figures 3B–3F; Movie S4). The observation that the D-V axis increases in length in mutant compared to control limbs cannot be explained by a decrease in cell proliferation. Thus, these quantifications indicate that limb elongation is impaired in $Wnt5a^{-/-}$; moreover, concomitant changes in the relative proportion of D-V and P-D axes suggest that this could be due to defects in oriented cellular events rather than to a defect in cell proliferation.

To determine whether cell organization is disrupted in limb of $Wnt5a^{-/-}$ embryos, we took advantage of a mouse strain carrying a ubiquitously expressed *GFP* transgene inserted on the X chromosome [12]. Because the X chromosome is randomly inactivated, female heterozygous embryos express GFP in a mosaic manner, allowing one to distinguish cell shape and follow cell behavior [13]. We found that in WT $Wnt5a^{+/+}$; $XGFP^{+/-}$ E9.25 embryos, mesenchymal cells of the limb were elongated toward the ectoderm as in chick embryos (Figures 3G and 3H; Figure S1). However, in mutant $Wnt5a^{-/-}$;$XGFP^{+/-}$ embryos, cells were not elongated and did not display any oriented protrusions (Figures 3J and 3K). This result was also confirmed via scanning electron microscopy (Figure S1). We next tracked the behavior of these cells via live-imaging two-photon microscopy as described above. We found that, as in the chick, in WT $XGFP^{+/-}$ embryos, cells displayed oriented movements and moved toward the overlying distal ectoderm

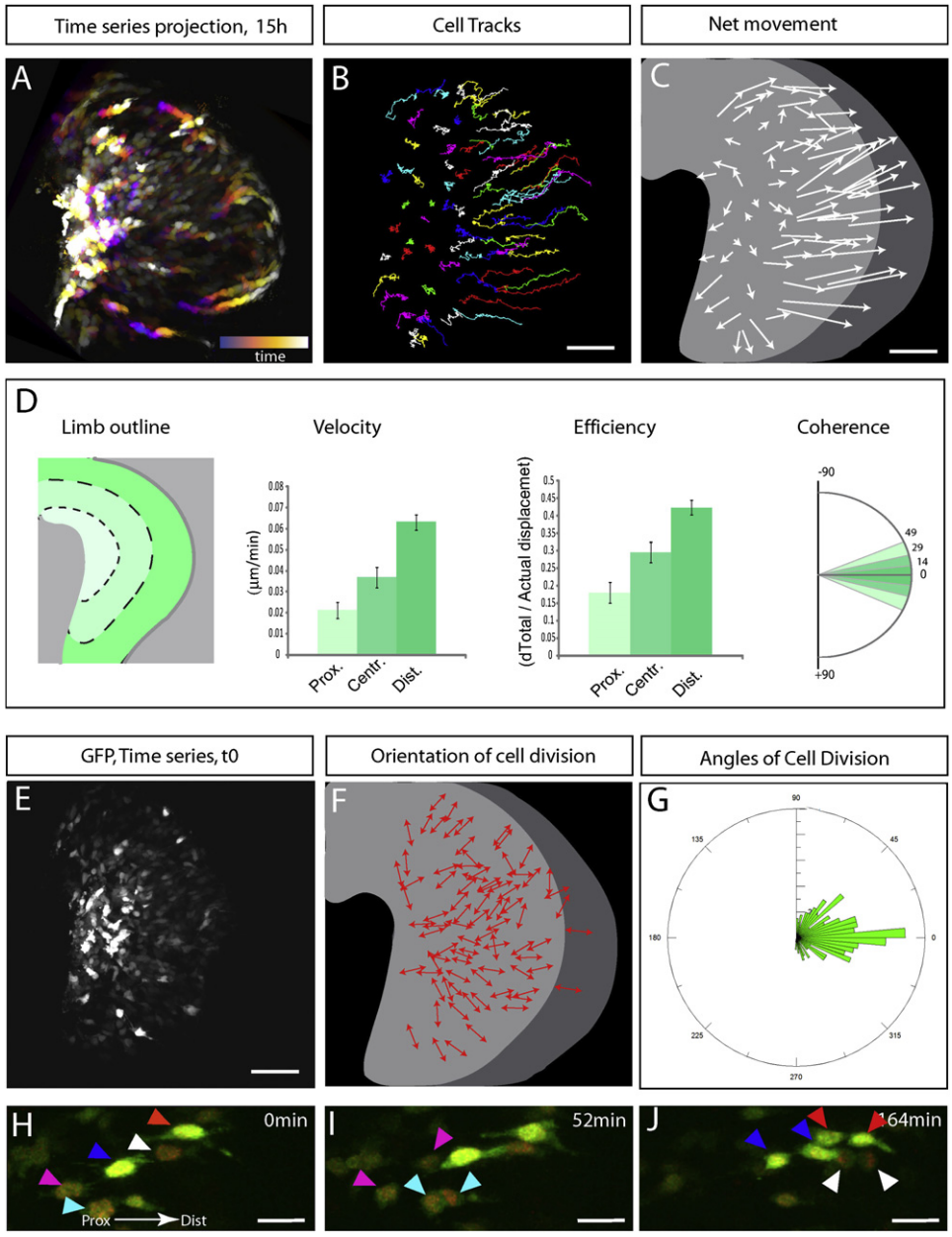

Figure 2. Cells of the Limb Exhibit Oriented Cell Movements and Oriented Cell Division

(A) Projection of a 15 hr time series view (corresponding to Movie S2) of a limb explant of a *GFP*-electroporated chick embryo. The projection is color coded: early times series are displayed in blue, and late time series are progressively displayed in orange and then white as the time-lapse experiment progresses as indicated by the bar at lower right.

(B) Cell tracks from time-lapse experiment in (A) (colors were randomly chosen). Cells were manually tracked.

(C) Schematic representing for each cell tracked in (B) the net movement (as shown by the length of each arrow) and the direction (as shown by the arrowheads).

(D) Quantification of cell velocity (in μm/min; second panel), efficiency (i.e., ratio between the distance between t_0 and t_f and the distance covered by the whole track; third panel) and coherence (i.e., standard deviation in angle of two cell directions within a range of 50 μm; fourth panel) in three arbitrarily subdivided areas (represented by shades of green) along the P-D axis (as schematized in the first panel).

(E) View of the first time series (t = 0) from the experiment presented in (A).

(F) Schematic representing the orientation of each cell (red arrows) that divided during the course of the time-lapse experiment in (A). (See Movie S2.)

(G) Quantification of the angle between the P-D axis of the limb bud and the axis of cell division. Angle of each cell division is shown on a unidirectional rosette graph divided in bins of 5°. Each interval on the radial axis represents 1% of cells per bin. Quantifications were made for a total of n = 331 cell divisions in five embryos.

(H–J) Time series at t = 0 (H), t = 52 min (I), and t = 164 min (J) of a time-lapse experiment (Movie S3) showing preferential P-D cell division at the distal end of the limb bud. The colored arrowheads indicate coelectroporated cells with both a *GFP* (in green) and *H2bRFP* (in red) construct and their progeny (same arrowhead color).

Scale bars represent 50 μm in (B), (C), and (E) and 20 μm in (H)–(J). Error bars represent standard error of the mean.

(Figures 3G–3I; Movie S4). Again similar to the chick, cell movements exhibited a proximal-to-distal gradient in velocity, efficiency, and coherence (Figure 3M). In *Wnt5a*$^{-/-}$;*XGFP*$^{+/-}$ embryos, cells located in the vicinity of the AER moved toward the ectoderm with a coherence comparable to that observed in WT embryos; however, they moved at reduced velocity and reduced efficiency compared to control cells (Figure 1M). In contrast, cells located in the dorsal and ventral domains of the limb bud exhibited disorganized movements with lower velocity, efficiency, and coherence than in WT limbs (Figures 3J–3M; Movie S5).

We then tested whether WNT5A is able to change the orientation of cells of the limb when expressed ectopically. We found that when DF1 cells expressing *Wnt5a* were implanted in *GFP*-electroporated limbs of chick embryos, *GFP*-labeled cells around the graft were elongated and intermingled with the cells expressing the ectopic *Wnt5a* (Figure 3N). Live imaging showed that limb cells located around the source of WNT5A rapidly changed their orientation and intercalated in between *Wnt5a*-expressing cells through highly coherent and efficient movements (Figures 3P, 3Q, and 3T; Movie S6). This behavior was not observed when control DF1 cells were implanted. Cells did not show any sign of reorientation and moved normally toward the ectoderm (Figures 3R and 3S; Movie S6). Thus, taken together, these results indicate that WNT5A is able to orient cells of the limb mesenchyme and that endogenous WNT5A is at least in part responsible for the observed oriented movements in the limb mesenchyme.

Wnt5a Regulates Oriented Cell Division in the Limb Bud

We next examined orientation of cell division in *Wnt5a* mutant limb buds. To this end, we performed a time-lapse experiment on mouse embryos ubiquitously expressing a transgene coding for a fusion between the human histone H2B and GFP proteins [14]. Similar to chick embryos, we observed that in WT *H2bGFP* E9.5 mouse embryos, cells divided in the direction of the overlying ectoderm (Figures 4A–4E; Movie S7). Quantification of the angle of cell divisions demonstrated a strong bias along the P-D axis (n = 1071 cell divisions; Figure 4F). In *Wnt5a*$^{-/-}$;*H2bGFP* embryos, cells located distally divided in the direction of the overlying ectoderm, as observed in WT embryos (Figures 4G–4K). However, cell divisions occurring in dorsal and ventral domains of the limb bud were disorganized. As a result, the overall distribution of the angle of cell divisions revealed a significantly weaker P-D bias (n = 791 cell divisions, χ^2 = 93.943, degrees of freedom = 35, $p < 0.00001$; Figure 4L; Movie S7). Thus, *Wnt5a* regulates at least partially the orientation of cell division within limb mesenchymal cells. Altogether, these data demonstrate that *Wnt5a* contributes to the control of limb bud elongation by regulating oriented movements and oriented cell division in the limb mesenchyme. The preferential loss of oriented cellular processes in the dorsal and ventral domains of *Wnt5a* mutant limb buds is consistent with the increase in the D-V axis in these mutants; however, the fact that there is still some P-D elongation in the absence of *Wnt5a* suggests that there may be some redundancy in the system.

JNK Acts Downstream of WNT5A in Oriented Cell Processes

The noncanonical WNT/PCP pathway has been shown to lead to changes in gene expression through activation of c-Jun N-terminal kinase (JNK), and WNT5A has been shown to induce JNK activation [15, 16]. We therefore tested whether direct modulation of JNK might have a stronger effect than WNT5A itself by examining orientation of cell division following inhibition of JNK activity. We cultured chick embryo explants coelectroporated with GFP and H2BRFP fusion protein in the presence of the JNK inhibitor SP600125 and live imaged cell behavior (Figures 4M–4O). We quantified the angle of cell divisions (n = 191 cell divisions) and found that in presence of SP600125, the planes of cell division were totally disorganized (Figure 4P). Time-lapse experiments also showed disorganized cell movements. Although SP600125-treated cells generally moved toward the distal end of the limb bud, these cells generated protrusions in many directions and exhibited much lower coherence and efficiency than controls (Figure 4Q). Thus, JNK activity is required to orient cell division and cell movement in the limb mesenchyme.

FGF Signaling Is Required for Cell Movement but Does Not Drive Cell Orientation

The FGF signaling pathway plays major roles during limb development. Moreover, FGF family members are expressed distally in the limb bud, and previous studies have suggested that FGF activity can act as a chemoattractant in the limb [17]. We therefore decided to reinvestigate its functions in light of the cellular events described above. Although at later stages FGF signaling is found in a narrow distal stripe, *Fgf8* is initially expressed in a broad domain in the distal ectoderm (Figure 5A) and only later becomes restricted to the AER. Thus, in principle, FGF activity could contribute to the oriented processes along the dorsal and ventral margins of the early limb bud as well as at the distal tip. Moreover, as previously described, we found that ERK/MAPK, a downstream effector of FGF signaling, displays a graded phosphorylation with high intensity at the distal tip and low intensity at the proximal end, reflecting the extent of the FGF pathway in the mesenchyme (Figures 5B and 5C) [18]. This is strikingly similar to the gradient in cell movement that we observed in the limb (Figure 5C).

To investigate its role in the movement of limb cells, we interfered in several ways with the FGF/MAPK pathway. First, we electroporated the limb mesoderm with dominant-negative and constitutively active forms of *Mek1* [19], which acts upstream of *Erk/Mapk*. In dominant-negative *Mek1*-electroporated embryos, cells were not as elongated as in controls and exhibited a great number of very thin cellular protrusions resembling filopodia (Figures 5F and 5G). Importantly, the cells were not misoriented, suggesting that the MAPK pathway does not regulate orientation. Conversely, cells expressing the constitutively active form of *Mek1* were elongated and exhibited thick cellular extensions resembling lamellipodia (Figures 5D and 5E). Lamellipodia are characteristic of motile cells and are believed to be the motor pulling cells forward during movement, whereas filopodia are characteristic of sensory functions. Thus, this result suggested a role for the FGF pathway in modulating motility of limb cells. Live imaging revealed that when MEK1 was inhibited with the specific inhibitor U0126, cells moved at a much lower velocity than control cells but in the appropriate orientation (Figures 5H–5J and 5Q; Movie S8). A similar effect was observed with either the FGFR1 inhibitor SU5402 or the dominant-negative form of *Mek1* (Figure S2). Moreover, we did not observe any defects in the orientation of cell division when limb buds were treated with U0126 as compared to control limb buds (data not shown). However, when the constitutively active *Mek1*

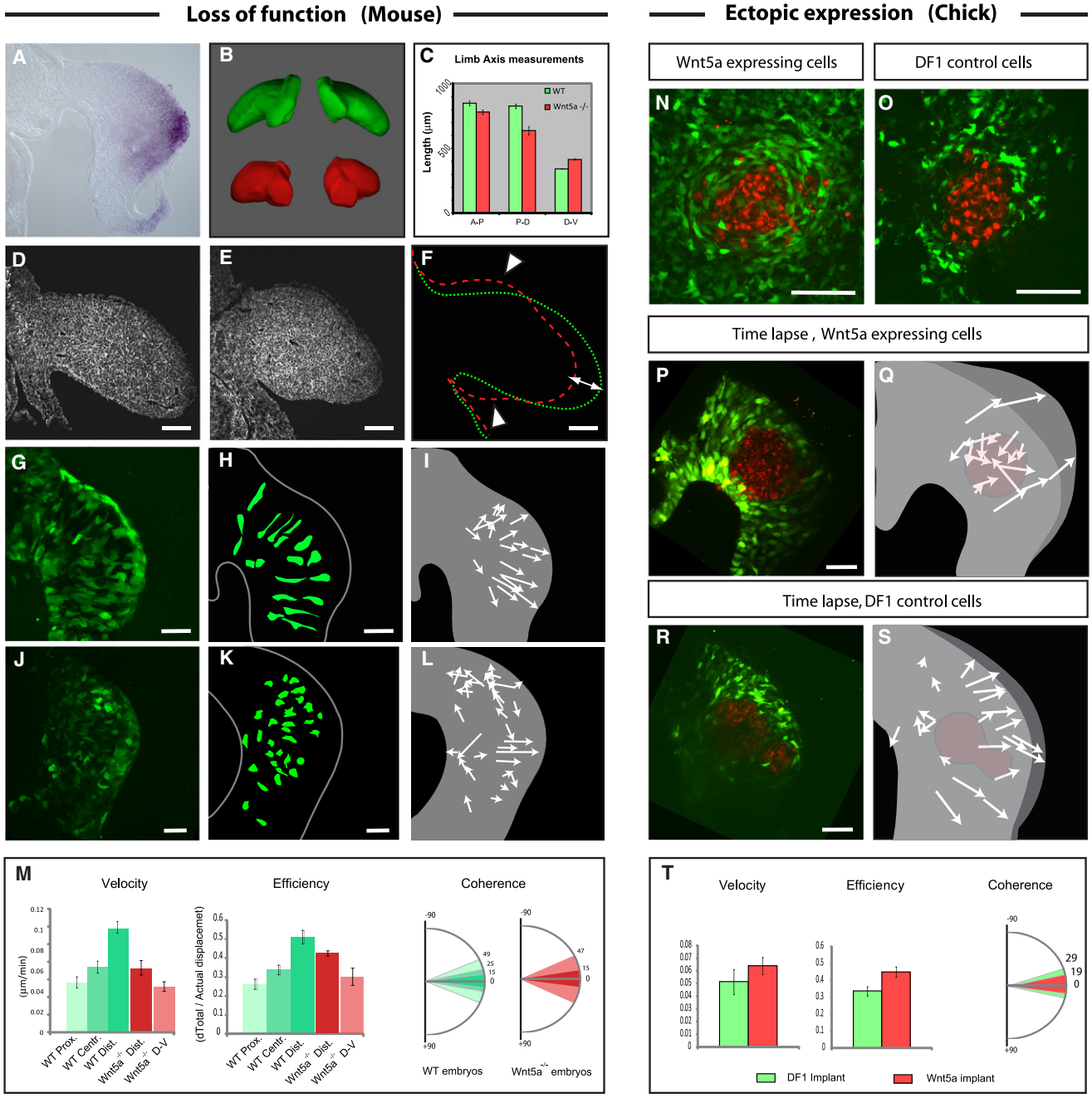

Figure 3. *Wnt5a* Regulates Limb Bud Elongation and Cell Orientation in the Mouse

(A) *Wnt5a* expression detected by in situ hybridization showing higher expression in the distal mesenchyme of the early limb bud.

(B) Wild-Type (WT) (green) and *Wnt5a*$^{-/-}$ mutant limb buds (red) reconstructed and virtually dissected from OPT acquisitions of E10.5 mouse embryos. *Wnt5a*$^{-/-}$ limbs exhibit elongation defects and appear roundish as compared to control. (See Movie S4.)

(C) Measurements (in µm) of the A-P (left bars), D-V (central bars), and P-D (right bars) axes lengths in WT (green bars) and *Wnt5a*$^{-/-}$ (red bars) embryos.

(D and E) Transverse sections of WT (D) and *Wnt5a*$^{-/-}$ (E) mouse embryos at E10.5 stained with phalloidin (in white).

(F) Outline of the WT (in green) and *Wnt5a*$^{-/-}$ (in red) limb buds shown in (D) and (E), respectively, showing the effect of loss of *Wnt5a* on the relative proportions of the limb bud (i.e., A-P axis, white arrowheads; P-D axis, white arrow).

(G and J) Transverse sections of WT *XGFP*$^{+/-}$ (G) and *Wnt5a*$^{-/-}$;*XGFP*$^{+/-}$ (J) mouse embryos at E9.25 showing the shape of *GFP*-expressing cells.

(H and K) Schematics representing outlines of *GFP*-expressing cells from sections shown in (G) and (J).

(I and L) Schematics showing net movement (arrow length) and direction (arrowheads) of cells during time-lapse experiments performed in WT *XGFP*$^{+/-}$ (I) and *Wnt5a*$^{-/-}$;*XGFP*$^{+/-}$ (L) mouse embryos at E9.25. (See Movie S5.)

(M) Quantification of cell velocity (first panel), efficiency (second panel), and coherence (third panel) in the proximal, central, and distal regions of the WT mouse limb bud (represented by shades of green as schematized in the first panel of Figure 2D) and in the most distal and dorsal-ventral parts of *Wnt5a*$^{-/-}$ mouse limb buds (dark red and light red, respectively).

(N and O) Transverse section of chick limb buds electroporated with a *GFP* construct (in green) and implanted with control (O) or *Wnt5a*-expressing (N) DF1 cells stained with DiI (in red).

construct was electroporated, cells displayed an exaggerated motile behavior with a much higher velocity than control cells. The original gradient of velocity observed in control *GFP* electroporation was lost when cells expressed the constitutively active *Mek1* form (Figures 5K–5M and 5Q; Movie S8). These data indicate that the FGF/MAPK pathway acts to promote cell movements.

In order to further understand the cellular events driven by FGF signaling, we exposed proximal cells of the limb, which are not normally exposed to FGF signaling, to an ectopic source of FGF8. In such limbs, proximal cells displayed higher velocity than in control limb buds (Figures 5N–5Q; Movie S8). Interestingly, as these proximal cells moved, they very rapidly invaded the source of FGF8, provoking elongation of the mesenchyme toward the proximal end of the limb bud. A similar effect was observed when beads soaked in FGF8 or DF1 cells expressing FGF8 were applied (Figures 5N–5P; Movie S8; Figure S2). These results are consistent with FGF8 acting as a chemoattractant for limb mesenchymal cells, as previously suggested [17]. Strikingly, however, in spite of the localized source of FGF, the movements induced by FGF8 displayed no obvious constant orientation. Cells extended a high number of protrusions, but in no particular direction, and frequently changed direction as they were moving. Moreover, cells showed very poor coherence and poor efficiency, revealing a low degree of organization in their movement (Figure 5Q). Thus, FGF8 is not able to orient mesenchymal cells of the limb. This is in net contrast with results obtained when *Wnt5a*-expressing cells are implanted in the limb bud. In this situation, cells display very organized movements exhibiting high coherence and high efficiency as they move toward the source of WNT5A (Figures 3P and 3Q). These results suggest that FGF8, unlike WNT5A, does not actually chemoattract surrounding cells by inducing oriented movements but instead acts to increase the velocity of random movements of these cells. Because the velocity of these random movements appears to be biased perhaps proportionally to the concentration of FGF8, cells eventually move closer to the source of FGF8 through mass action. Altogether, these results demonstrate that FGF signaling is dispensable for cell orientation in the limb but is required to induce a gradient of cell movement that is necessary to drive limb bud elongation.

Discussion

Taken together, our data suggest that orientation of cell division and cell movements is sufficient to explain the oriented growth of the limb bud. As this manuscript was in preparation, Boehm et al. published a study directly testing the alternative proliferation rate model [20]. The authors combine biological measurements with computational modeling and conclude that such a model is not realistic. They therefore propose that the limb elongates through oriented cell events, such as oriented cell division and oriented cell movements. This study is in agreement with our present findings and supports our model.

In a second related study published as this manuscript was in preparation, Wyngaarden et al. investigated tissue movement at the onset of limb bud formation. They found that the limb bud initiates its formation along the A-P axis by recruiting lateral plate mesoderm cells via rostral-to-caudal movement of tissue and cell divisions [21]. Similar to the morphogenic processes elucidated here, these movements involve oriented cellular properties regulated at least in part by *Wnt5a*.

We examined subsequent steps of limb morphogenesis and showed that WNT5A and JNK activity are required to drive proper limb morphogenesis, acting to orient cellular processes including mitosis and directional cell movements. In cell culture, WNT5A has been shown to bind to ROR2 (an orphan tyrosine kinase receptor) and to activate JNK [15]. Consistent with our in vivo results, WNT5A/ROR2 activity induces polarized cell migration and reorientation of the microtubule-organizing center in a JNK-dependent manner in vitro. Moreover, mice mutant for *Ror2* and double mutants for *Ror1* and *Ror2* exhibit phenotypes very similar to *Wnt5a* mutant mice [22, 23].

The FGF signaling pathway has been shown to be important in driving cell proliferation, cell survival, and specification of limb mesenchymal cells. Our study indicates that an additional role of FGF activity is to promote the velocity of cell movements within the limb bud, thereby promoting its elongation. Consistent with this, conditional inactivation of *Fgfr1* in the limb mesoderm disrupts the relative proportions of the limb bud and consequently of the skeletal elements [24]. In these mutants, the length of the P-D axis is reduced whereas the D-V and A-P axes are expanded. Strikingly, the same result was obtained by applying FGF4 beads to the developing limb [17]. Here we have shown that the effect of FGF/MAPK signaling emanating from the AER is different than the effect induced by WNT5A in the limb bud. Whereas WNT5A induces directional movement of cells, FGF8 acts to induce rapid albeit disorganized movements. However, like WNT5A, FGF activity ultimately results in distal elongation. These observations suggest that FGF8 acts by inducing random movements, but with a higher velocity as cells move close to the source. As this manuscript was in preparation, a study by Bénazéraf et al. proposed that the FGF pathway drives tail bud elongation in the chick embryo by promoting random cell movements [25]. They suggest that FGF creates a gradient of cell motility and that the tail bud elongates by mass action of random cell movement at the posterior end of the embryo. Although our data indicate a similar mode of FGF action, cells in the limb bud additionally undergo oriented processes of cell division and directional movements under the influence of WNT5A. Our study indicates that it is the combined action of noncanonical WNT and FGF that integrates orientation and movement, consequently driving limb bud elongation and thereby establishing a progenitor field of the proper

(P and R) First time series (t = 0) from time-lapse experiments (Movie S6) showing control DF1 cells (R, in red) or *Wnt5a*-expressing cells (P, in red) implanted in limb buds previously electroporated with a *GFP* construct (in green).

(Q and S) Schematics showing net movement (arrow length) and direction (arrowheads) of *GFP*-expressing cells from (P) and (R). *GFP*-expressing cells move toward the source of WNT5A in (Q) and move normally toward the ectoderm in (S). The position of control DF1 cells (S) and *Wnt5a*-expressing cells (Q) is indicated in red. (See Movie S6.)

(T) Quantification of cell velocity (first panel), efficiency (second panel), and coherence (third panel) of *GFP*-labeled cells surrounding implanted DF1 cells (green) or *Wnt5a*-expressing cells (red).

Scale bars represent 50 μm. Error bars represent standard error of the mean.

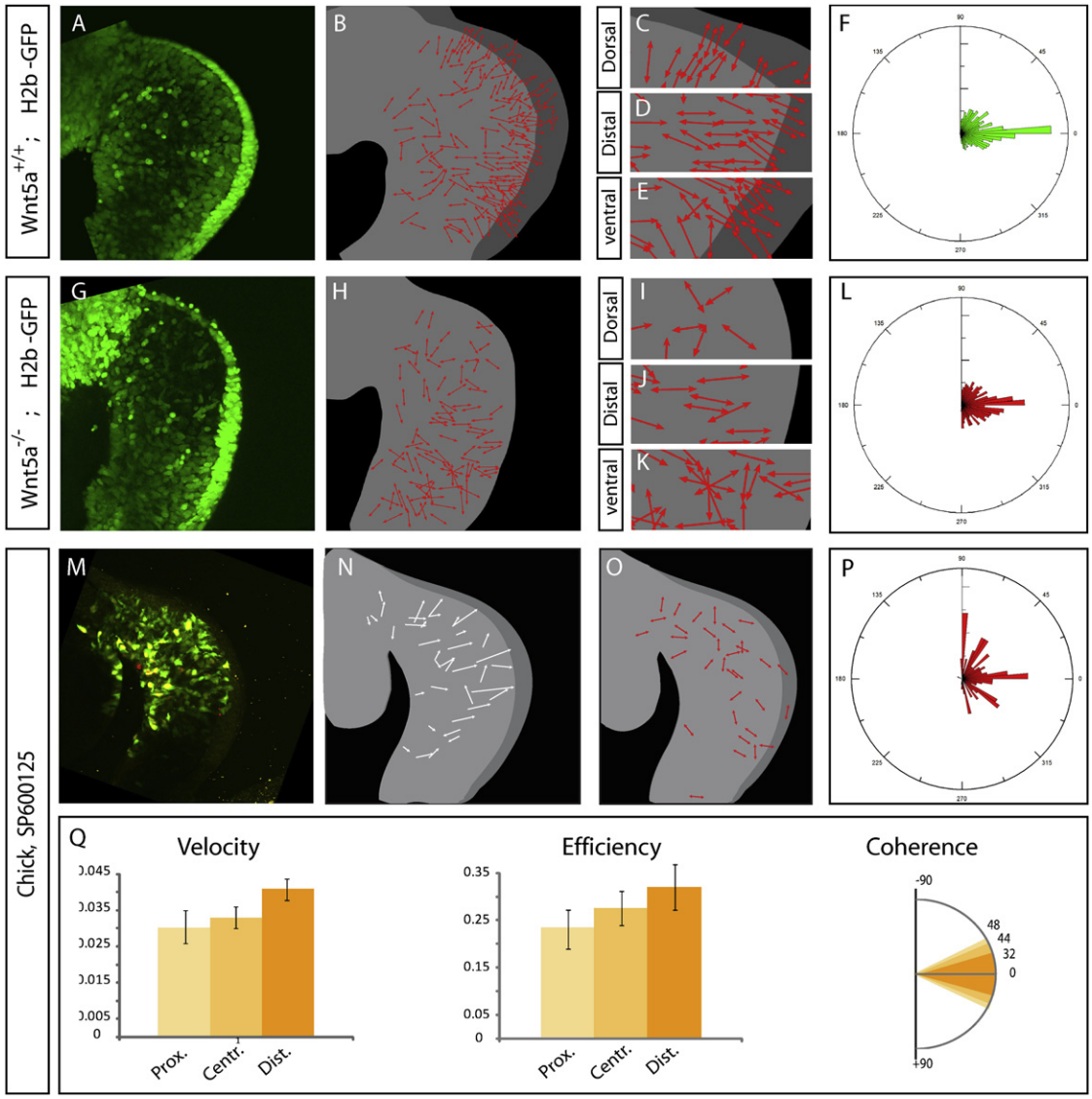

Figure 4. WNT5A/JNK Regulates Orientation of Cell Division

(A and G) First time series (t = 0) of time-lapse experiments (Movie S7) in limb buds of WT *H2bGFP* (A) or *Wnt5a*$^{-/-}$;*H2bGFP* (G) mouse embryos at E9.5.

(B and H) Schematics representing the orientation of cell division (red arrows) from time-lapse experiments in (A) and (G), respectively.

(C–E and I–K) Enlargements of the dorsal (C and I), distal (D and J), and ventral (E and K) areas showing regional differences in the orientation of cell divisions.

(F, L, and P) Quantifications of the angle between the P-D axis and the axis of cell division identified from the time-lapse experiments performed in WT *H2bGFP* (F) and *Wnt5a*$^{-/-}$;*H2bGFP* (L) mouse embryos at E9.5 and chick limb buds treated with the JNK inhibitor SP600125 (P), as shown in (A), (G), and (M), respectively. The rosette graph is divided in bins of 5°. Each interval on the radial axis represents 5% of cells per bin.

(M) First time series (t = 0) from a time-lapse experiment (see Movie S7) in chick limb bud explants electroporated with *GFP* (green) and *H2bRFP* (red) constructs and cultured in presence of the JNK inhibitor SP600125.

(N) Schematic showing net movement (arrow length) and direction (arrowheads) of cells shown in (M).

(O) Schematic representation of the direction of cell division (red arrows) shown in (M).

(Q) Quantification of cell velocity (first panel), efficiency (second panel), and coherence (third panel) in the proximal, central, and distal regions (represented by shades of color [orange] as schematized in the first panel of Figure 2D) of chick limbs treated with SP600125. Error bars represent standard error of the mean.

dimensions for the subsequent patterning and morphogenesis of limb anatomy.

Supplemental Information

Supplemental Information includes two figures, Supplemental Experimental Procedures, and eight movies and can be found with this article online at doi:10.1016/j.cub.2010.09.063.

Acknowledgments

We thank Carla Kim, Andy McMahon, Elaine Fuchs, Rudolf Jaenisch, and Andras Nagy for sharing mouse strains and Andrew Russell for assistance with statistical tests. J.G. is a fellow of the Human Frontier Science Program. C.V is supported by National Institutes of Health (NIH) grants UO1-HL080731, PO1-AI05490, and RO1-EB006432. This work was supported by NIH grant R01-HD045499 to C.J.T.

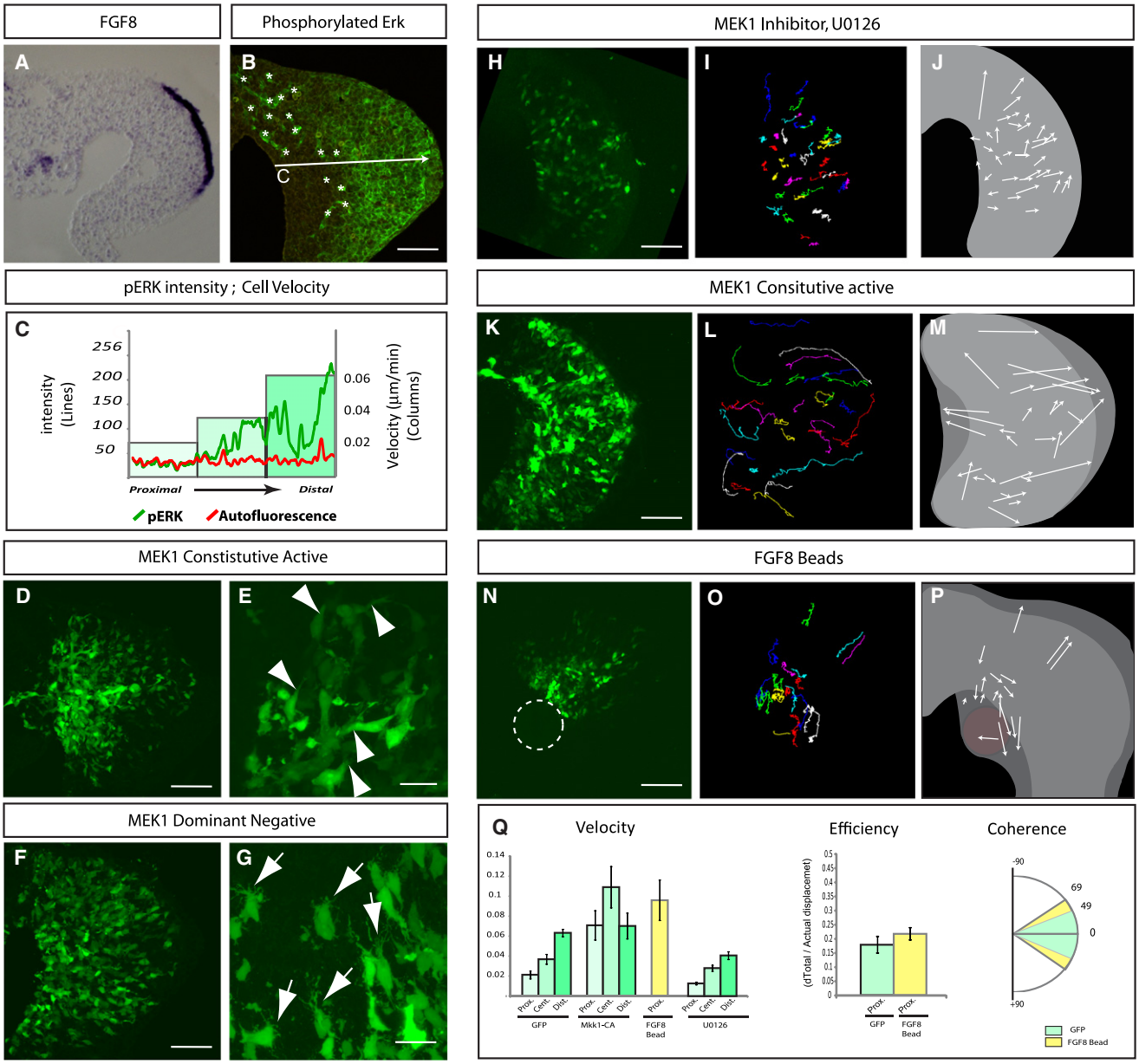

Figure 5. FGF/MAPK Signaling Promotes Cell Movement

(A) Transverse section showing FGF8 expression detected by in situ hybridization in the distal ectoderm of a chick limb bud.
(B) Transverse section of a limb bud stained with a phosphorylated-ERK/MAPK antibody.
(C) Intensity profile of pERK (green line) and nonspecific red autofluorescence (red line) along the P-D axis of the limb as shown in (B) correlated with the velocity of cells from the proximal, central, and distal regions of the limb bud (columns) as shown in Figure 2D.
(D) Transverse section of chick limb bud coelectroporated with constitutively active *Mek1* (CA-MEK1) and *GFP* constructs.
(E) High magnification showing lamellipodia of electroporated *GFP*-expressing cells (arrowheads).
(F) Transverse section of chick limb bud coelectroporated with dominant-negative *Mek1* and *GFP* constructs.
(G) High magnification showing filopodia protruding from cells electroporated with dominant-negative *Mek1* and *GFP* (arrows).
(H, K, and N) First time series (t = 0) of time-lapse experiments (Movie S8) on chick limb buds electroporated with constitutively active *Mek1* and *GFP* (K), *GFP* only and cultured in presence of the MEK1 inhibitor U1026 (H), or *GFP* only and cultured with a bead soaked in FGF8 (N). (See Movie S8.)
(I, L, and O) Cell tracks from time-lapse experiments shown in (H), (K), and (N), respectively.
(J, M, and P) Schematics representing net movement (arrow length) and direction (arrowheads) of cells tracked in (I), (L), and (O), respectively.
(Q) Left graph: quantification of velocity (in µm/min) of cells electroporated with *GFP* only (leftmost group of three bars), with constitutively active *Mek1* (middle group of three bars), or in the presence of FGF8 beads (yellow bar) or U0126 (rightmost group of three bars) within the proximal, central, and distal regions of the limb bud (represented by shades of green as in Figure 2D). Center graph: quantification of efficiency of proximal cells of the limb electroporated with *GFP* only or in the presence of a FGF8 bead (yellow). Right graph: quantification of coherence of movement of cells located within the proximal region of the limb bud electroporated with *GFP* (green) or exposed to FGF8 beads (yellow). Error bars represent standard error of the mean.
Scale bars represent 50 µm in all panels except (E) and (G), where they represent 10 µm.

Received: July 12, 2010
Revised: September 6, 2010
Accepted: September 28, 2010
Published online: November 4, 2010

References

1. Ede, D.A., and Law, J.T. (1969). Computer simulation of vertebrate limb morphogenesis. Nature *221*, 244–248.
2. Dillon, R., and Othmer, H.G. (1999). A mathematical model for outgrowth and spatial patterning of the vertebrate limb bud. J. Theor. Biol. *197*, 295–330.
3. Morishita, Y., and Iwasa, Y. (2008). Growth based morphogenesis of vertebrate limb bud. Bull. Math. Biol. *70*, 1957–1978.
4. Hornbruch, A., and Wolpert, L. (1970). Cell division in the early growth and morphogenesis of the chick limb. Nature *226*, 764–766.
5. Ede, D.A., Flint, O.P., and Teague, P. (1975). Cell proliferation in the developing wing-bud of normal and talpid3 mutant chick embryos. J. Embryol. Exp. Morphol. *34*, 589–607.
6. Fernández-Terán, M.A., Hinchliffe, J.R., and Ros, M.A. (2006). Birth and death of cells in limb development: a mapping study. Dev. Dyn. *235*, 2521–2537.
7. Ulrich, F., Krieg, M., Schötz, E.M., Link, V., Castanon, I., Schnabel, V., Taubenberger, A., Mueller, D., Puech, P.H., and Heisenberg, C.P. (2005). Wnt11 functions in gastrulation by controlling cell cohesion through Rab5c and E-cadherin. Dev. Cell *9*, 555–564.
8. Tada, M., and Kai, M. (2009). Noncanonical Wnt/PCP signaling during vertebrate gastrulation. Zebrafish *6*, 29–40.
9. Gavin, B.J., McMahon, J.A., and McMahon, A.P. (1990). Expression of multiple novel Wnt-1/int-1-related genes during fetal and adult mouse development. Genes Dev. *4* (12B), 2319–2332.
10. Parr, B.A., Shea, M.J., Vassileva, G., and McMahon, A.P. (1993). Mouse Wnt genes exhibit discrete domains of expression in the early embryonic CNS and limb buds. Development *119*, 247–261.
11. Yamaguchi, T.P., Bradley, A., McMahon, A.P., and Jones, S. (1999). A Wnt5a pathway underlies outgrowth of multiple structures in the vertebrate embryo. Development *126*, 1211–1223.
12. Hadjantonakis, A.K., Cox, L.L., Tam, P.P., and Nagy, A. (2001). An X-linked GFP transgene reveals unexpected paternal X-chromosome activity in trophoblastic giant cells of the mouse placenta. Genesis *29*, 133–140.
13. Yen, W.W., Williams, M., Periasamy, A., Conaway, M., Burdsal, C., Keller, R., Lu, X., and Sutherland, A. (2009). PTK7 is essential for polarized cell motility and convergent extension during mouse gastrulation. Development *136*, 2039–2048.
14. Tumbar, T., Guasch, G., Greco, V., Blanpain, C., Lowry, W.E., Rendl, M., and Fuchs, E. (2004). Defining the epithelial stem cell niche in skin. Science *303*, 359–363.
15. Oishi, I., Suzuki, H., Onishi, N., Takada, R., Kani, S., Ohkawara, B., Koshida, I., Suzuki, K., Yamada, G., Schwabe, G.C., et al. (2003). The receptor tyrosine kinase Ror2 is involved in non-canonical Wnt5a/JNK signalling pathway. Genes Cells *8*, 645–654.
16. Schambony, A., and Wedlich, D. (2007). Wnt-5A/Ror2 regulate expression of XPAPC through an alternative noncanonical signaling pathway. Dev. Cell *12*, 779–792.
17. Li, S., and Muneoka, K. (1999). Cell migration and chick limb development: chemotactic action of FGF-4 and the AER. Dev. Biol. *211*, 335–347.
18. Corson, L.B., Yamanaka, Y., Lai, K.M., and Rossant, J. (2003). Spatial and temporal patterns of ERK signaling during mouse embryogenesis. Development *130*, 4527–4537.
19. Delfini, M.C., Dubrulle, J., Malapert, P., Chal, J., and Pourquié, O. (2005). Control of the segmentation process by graded MAPK/ERK activation in the chick embryo. Proc. Natl. Acad. Sci. USA *102*, 11343–11348.
20. Boehm, B., Westerberg, H., Lesnicar-Pucko, G., Raja, S., Rautschka, M., Cotterell, J., Swoger, J., and Sharpe, J. (2010). The role of spatially controlled cell proliferation in limb bud morphogenesis. PLoS Biol. *8*, e1000420.
21. Wyngaarden, L.A., Vogeli, K.M., Ciruna, B.G., Wells, M., Hadjantonakis, A.K., and Hopyan, S. (2010). Oriented cell motility and division underlie early limb bud morphogenesis. Development *137*, 2551–2558.
22. Takeuchi, S., Takeda, K., Oishi, I., Nomi, M., Ikeya, M., Itoh, K., Tamura, S., Ueda, T., Hatta, T., Otani, H., et al. (2000). Mouse Ror2 receptor tyrosine kinase is required for the heart development and limb formation. Genes Cells *5*, 71–78.
23. Nomi, M., Oishi, I., Kani, S., Suzuki, H., Matsuda, T., Yoda, A., Kitamura, M., Itoh, K., Takeuchi, S., Takeda, K., et al. (2001). Loss of mRor1 enhances the heart and skeletal abnormalities in mRor2-deficient mice: redundant and pleiotropic functions of mRor1 and mRor2 receptor tyrosine kinases. Mol. Cell. Biol. *21*, 8329–8335.
24. Verheyden, J.M., Lewandoski, M., Deng, C., Harfe, B.D., and Sun, X. (2005). Conditional inactivation of Fgfr1 in mouse defines its role in limb bud establishment, outgrowth and digit patterning. Development *132*, 4235–4245.
25. Bénazéraf, B., Francois, P., Baker, R.E., Denans, N., Little, C.D., and Pourquié, O. (2010). A random cell motility gradient downstream of FGF controls elongation of an amniote embryo. Nature *466*, 248–252.